Phys. Status Solidi C **6**, No. 8, 1862–1867 (2009) / **DOI** 10.1002/pssc.200881471

physica status solidi c
www.pss-c.com
current topics in solid state physics

Localisation and identification of recombination-active extended defects in crystalline silicon by means of focused ion-beam preparation and transmission electron microscopy

L. Stolze[1,2], P. Saring[1], C. Rudolf[1], and M. Seibt[1,*]

[1] IV. Physikalisches Institut der Georg-August-Universität Göttingen, Friedrich-Hund-Platz 1, 37077 Göttingen, Germany
[2] Now at: Q-Cells AG, Guardianstraße 16, 06766 Bitterfeld-Wolfen, Germany

Received 17 September 2008, revised 13 January 2009, accepted 14 April 2009
Published online 17 June 2009

PACS 61.72.Nn, 68.37.Hk, 68.37.Lp, 73.30.+y

* Corresponding author: e-mail seibt@ph4.physik.uni-goettingen.de, Phone: +49-551-394553, Fax: +49-551-394560

This paper reports on the localisation of extended defects related to the co-precipitation of transition metal impurities in silicon and their preparation for subsequent analysis using techniques of transmission electron microscopy (TEM). Two approaches are described, i.e. (i) localisation of recombination-active defects by light-beam induced current followed by preferential chemical etching and TEM sample preparation using focused-ion beam (FIB), and (ii) the replacement of the chemical etching by *in situ* Ga^+ irradiation in the FIB system. The former technique is successfully applied to copper-rich precipitate colonies in silicon whereas the latter proofs to be the superior approach for nickel-rich particles. Structural and chemical analyses using TEM techniques are described for both cases.

1 Introduction Electronic and optical properties of semiconducting materials are generally affected by the presence of extended defects of various and frequently unknown type. Examples range from dislocations killing VCSEL laser diodes to silicide precipitates and decorated dislocations in crystalline silicon for solar cells which are recombination-active and hence reduce minority carrier lifetime and solar cell efficiency. Structural and/or chemical analysis of such defects by microscopic techniques such as transmission electron microscopy (TEM) is frequently hampered or even impossible due to the low defect density. Recently, micro X-ray fluorescence spectroscopy (μ-XRF) in combination with X-ray absorption spectroscopy (XAS) has proven to be a powerful tool to chemically analyse transition metal related precipitates [1, 2]. Structural information of the underlying defect structures, however, can not be obtained by this technique. Hence, alternative approaches are needed to localise defects and produce electron-transparent samples from such regions.

In this work, we describe different approaches of delineating extended defects close to the surface of crystalline silicon, subsequent local preparation of TEM samples by focused ion-beam (FIB) in a FEI Nova Nanolab 600 dualbeam scanning electron microscope (SEM) followed by structural and chemical analysis by means of TEM.

Examples described in detail:

– localisation of recombination-active copper silicide colonies by means of light-beam induced current

(LBIC) imaging, subsequent delineation defect etching and final FIB preparation for TEM analyis,
– *in situ* delineation using grazing angle Ga^+ irradiation in the FIB which reveals plate-shaped precipitates with a low density; subsequent FIB preparation and TEM analyses show silicide platelets isomorphous to $NiSi_2$ containing nickel, silicon and up to 13at% copper

Especially the combination of imaging recombination-active extended defects by LBIC and defect etching with FIB preparation and subsequent chemical and structural analysis opens the route to experiments in the low-defect-density regime or even on single or isolated extended defects.

2 Experimental Two types of starting materials have been used in this study, i.e. bicrystals produced by wafer direct bonding of two n-type Czochralski grown silicon wafers and p-type float zone silicon. The former was diffused with nickel and copper and 1050 °C and subseqently cooled at 5 K/s to room temperature, as described in detail elsewhere [3]. The latter was first doped with nickel by in-diffusion at 1050 °C from an evaporated nickel film, quenched to room temperature, subsequently covered on one side with an evaporated copper film and finally annealed at 750 °C. For LBIC investigations, Schottky contacts were produced by Au evaporation on a freshly etched surface (for details, see [4]). The experimental setup uses a laser diode emitting at $\lambda = 850$ nm and allows measuring at temperatures down to 80 K. Preferential etching was performed using Secco etch for various times down to about 4 s [5].

TEM samples were prepared in a Nova NanoLab 600 using 30 kV Ga^+ ions for lamella definition, cut-out and thinning, and 5 kV Ga^+ ions for a final ion polishing. TEM investigations were performed at 200 kV in a Philips CM200-UT-FEG equipped with a Si:Li detector (Oxford Link ISIS) for X-ray spectrometry (EDX).

3 Results and discussion In this section we give a detailed description of two different approaches for the localisation of recombination-active extended defects and their subsequent preparation for TEM analyses using focused-ion beam, FIB. The first route described in Section 3.1 involves preferential etching and proved to be applicable to precipitate colonies formed by co-precipitation of copper and nickel under copper-rich conditions. The technique fails for $NiSi_2$:Cu platelets which are observed for co-precipitation under nickel-rich conditions. An alternative route which is successful in this case is described in Section 3.2.

3.1 Route 1: LBIC mapping and preferential etching It is known for a long time that copper typically precipitates in form of colonies consisting of planar arrangements of small Cu_3Si particles bordered by an edge dislocation loop [6]. Planar branches are found predominantly parallel to Si $\{110\}$ planes and occasionally parallel to $\{001\}$ planes. Fig. 1 is a LBIC micrograph of an isolated colony viewed along the Si[110] direction. Strong dark contrasts indicate the lines of intersection of a planar branch and the sample surface. It can be concluded that short branches parallel to Si($1\bar{1}0$) exist that are viewed edge-on (see label '1') in addition to larger branches on inclined Si$\{110\}$ planes labeled '2' and '3' in Fig. 1. The strong LBIC contrast further indicates that the main portion of the colony consists of a branch viewed *flat-on*, i.e. it runs parallel to the surface on the Si(110) plane which will be substantiated by the TEM analysis described below.

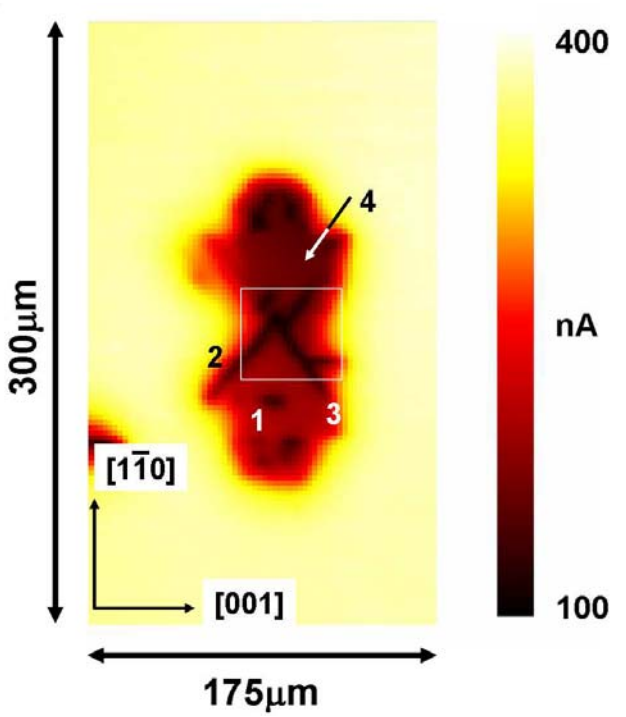

Figure 1 Room temperature LBIC map of a copper silicide colony which – according to TEM investigations – consists of planar arrangements of small precipitates parallel to Si$\{110\}$ planes. The projection is along the $[110]$ direction of the silicon indicating that branches parallel to Si($\bar{1}10$) ('1', viewed edge-on), Si(011) or Si($10\bar{1}$) ('2', inclined to the surface), Si($0\bar{1}1$) or Si(101) ('3', inclined to the surface), and parallel to Si(110) ('4', viewed flat-on); the rectangle in the centre indicates the position of the of the area shown in Fig. 2a.

After removing the Schottky contact by chemical etching in *aqua regia* the sample was etched for 4 s in Secco etch [5] subsequently rinsed in de-ionised water and mounted on a SEM holder. The secondary electron image (Fig. 2a) shows the resulting etch structures in the central region of the defect imaged in Fig. 1. The rectangular hatched area indicates the region of FIB preparation of a TEM lamella.

The inclined branch ('3' in Fig. 1) is imaged in the cross-section electron micrograph shown in Fig. 2b. Indi-

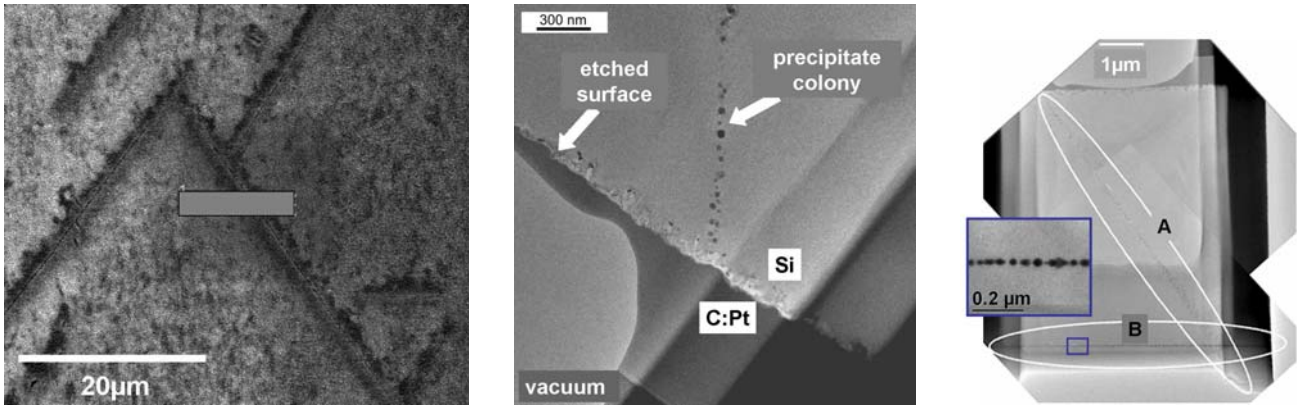

a) b) c)

Figure 2 (a) SEM micrograph showing the central part of the defect shown in the LBIC map of Fig. 1 after Schottky contact removal and short preferential etching; the rectangle indicates the location of the TEM lamella prepared by FIB. (b) TEM micrograph of the lamella indicating the etched surface and the colony branch labeled '3' in Fig. 1; C:Pt denotes the deposited composite consisting of amorphous C and crystalline Pt particles which serves as a protection during FIB preparation. (c) low-magnification TEM micrograph showing the whole lamella with an inclined colony (A) which corresponds to the colony labeled '3' in Fig. 1 and a planar branch parallel to the surface (B); the inset shows an enlarged image of the flat-on colony obtained from the part marked by the small rectangle.

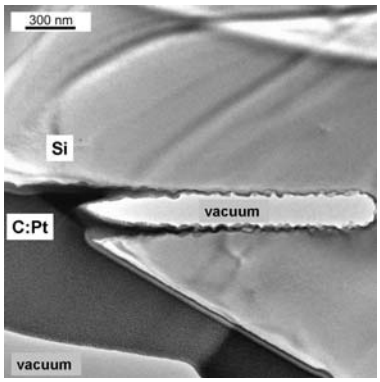

Figure 3 TEM micrograph of a $NiSi_2$:Cu precipitate prepared by the procedure described in Section 3.1; the platelet has been completely dissolved during etching leaving a hole in the silicon which is partly filled by the Pt:C cover of the FIB preparation.

vidual precpitates along a line inclined to the surface are clearly seen in addition to the rough preferentially etched surface. The line of precipitates is along $[11\bar{1}]$ so that a copper particle colony parallel to Si(101) planes can be concluded for the branch labeled '3' in Fig. 1.

If the whole FIB-prepared TEM lamella is imaged the colony branch parallel to the surface is revealed at a depth of about 7 m. This is shown in Fig. 2c where the inclined branch is labeled 'A' and 'B' indicates the branch parallel to the surface. Hence, the interpretation of the LBIC contrast given above as being due to a colony branch viewed *flat-on* has been proven experimentally.

Co-precipitation of nickel and copper under nickel-rich conditions leads to the formation of silicide platelets consisting of a solid solution of Cu in $NiSi_2$, subsequently referred to as $NiSi_2$:Cu. Using route 1 for TEM sample preparation successfully localises the defects. FIB preparation and TEM, however, shows that in this case major parts of the defects are removed by the preferential etching. Figure 3 is a TEM bright-field micrograph mainly showing a deep trench-like hole in the silicon. It is interesting to note that the deep etch pit is effectively plugged by the Pt:C cover used in the FIB preparation process.

3.2 Route 2: *In situ* ion irradiation For such defects, an alternative technique (route 2) can be successfully applied. In this case, ion irradiation is used as a means of preferential etching producing surface features visible in the SEM. Here, we describe a technique which includes *in situ* ion irradiation in the FIB/SEM machine using 30 kV Ga^+ ions incident under 62 ° to the surface normal. Typical conditions use an ion current of 20 nA which results in sputtering rates of 4.3 nm/s for silicon. The irradiated area is on the order of $50 \times 100\ \mu m^2$ and typical irradiation times are 30 s between successive inspection of the sputtered region by SEM. This is equivalent to inspecting a volume of about $650\ \mu m^3$ for a defect giving rise to visible surface features with each SEM imaging. Hence, on the average one defect should be visible every 30 s for a volume density of $1.6 \times 10^9\ cm^{-3}$ which is already difficult to access by traditional TEM sample preparation methods.

Figure 4a is a SEM image showing two surface features with a typical size of a micrometer indicated by arrows. The rectangular region on the left hand side is shown at higher magnification in the inset. Both features exhibit a rod-like shape which would be consistent with the intersection of a planar defect on Si{111} planes with the [110]-oriented sample surface. The plate-shaped defect can in fact be observed if a TEM sample is prepared from

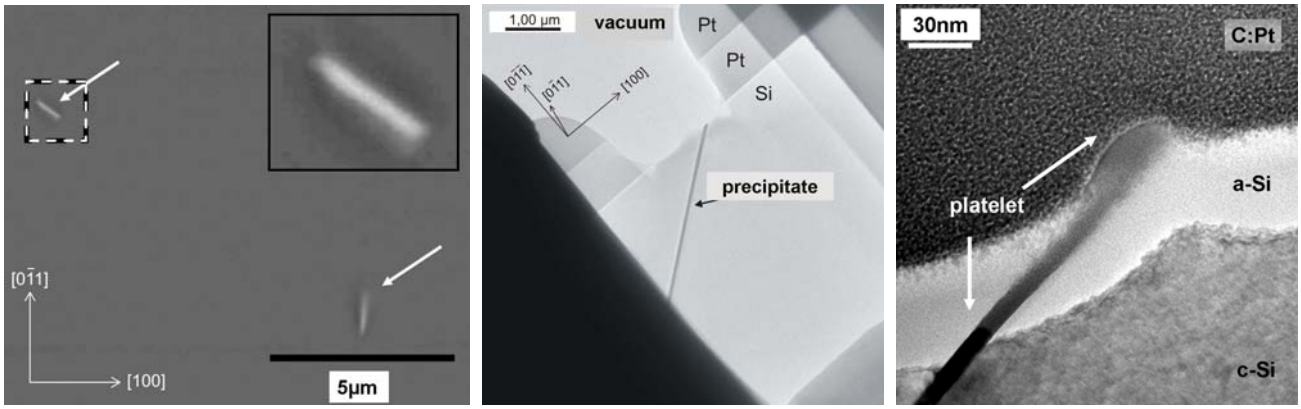

a) b) c)

Figure 4 Course of TEM sample preparation using route 2: (a) SEM micrograph showing two contrasts (arrows) after Ga^+ irradiation; the inset shows an enlarged image of the area marked by the dashed rectangle. (b) low-magnification TEM micrograph of the prepared lamella containing one plate-shaped precipitate. (c) TEM image of the platelet intersecting the surface and forming a small protrusion which contributes to the SEM contrast seen in (a); a top layer with a thickness of about 50 nm has been amorphised due to Ga^+ irradiation (a-Si).

the region of such surface features. Figure 4b is a low-magnification bright-field micrograph of a major of the TEM lamella. The dark line inclined with respect to the surface shows a plate-shaped precipitate on Si$\{111\}$ planes which is viewed *edge-on* in the [0$\bar{1}$1] oriented foil.

A TEM image of the top part of the precipitate is shown in Fig. 4c which reveals some interesting features related to the delineation process by ion irradiation. The speckle-like contrast in the upper part is due to the C:Pt cover which consists of small nm-sized Pt particles embedded in amorphous carbon. The bright region consists of silicon according to EDX analysis and exhibits amorphous diffraction rings. Hence, an approximately 50 nm thick surface layer of the silicon has been amorphised by the Ga^+ irradiation at 30 kV. It can further be seen that the $NiSi_2$:Cu platelet protrudes the original surface from which a slightly lower sputtering yield of the precipitate compared to the silicon matrix can be concluded. Furthermore, the platelet is severely damaged in the part embedded in the a-Si layer and a slight swelling seems to occur where the $NiSi_2$:Cu precipitate has been exposed to the Ga^+ beam; the latter is now encompassed by the C:Pt cover used in the course of FIB preparation.

For the example presented here, the chemical composition of the precipitates is important if a quantitative understanding of metal impurity co-precipitation is to be developed. Hence, the defects have been analysed by *energy dispersive x-ray spectrometry, EDX*. Figure 5 shows elemental maps of silicon (Fig. 5a), nickel (Fig. 5b), and copper (Fig. 5c), where the quantity

$$f_X = \frac{k_X \cdot I_X}{k_{Si}I_{Si} + k_{Ni}I_{Ni} + k_{Cu}I_{Cu}} \qquad (1)$$

is displayed. The symbol k_X refers to the k-factor of the investigated chemcial species (X = Si, Ni, Cu) which is used in standard Cliff-Lorimer analysis [7] and I_X denotes the number of counts measured for these species. This quantity f_X is close to the mole fraction of each element; due to the contribution of the bremstrahlung background, however, there is a systematic error, especially for copper whose concentration is rather small. Hence, the color code should be taken as a semi-quantitative indication of the composition.

The first observation is related to the top part of the platelet which has been exposed to the 30 kV Ga^+ beam during defect delineation. Figures 5a and 5b show a reduced silicon concentration at the expense of an increased nickel concentration. The profile along the line labeled 'A' in Fig. 5b is shown in Fig. 6a furthermore indicates that the copper concentration is not affected here. Simulations using the standard SRIM code [8,9] in fact reveal an enhanced sputtering yield of silicon compared to nickel. Hence, it has to be concluded that the change of composition in this top part of the defect is due to selective sputtering during defect delineation.

The remaining part of the platelet has an almost homogeneous composition which is close to $Ni_{0.31}Si_{0.64}Cu_{0.05}$ as is deduced from background-corrected EDX spectra combined with standard Cliff-Lorimer analyses [7]. In order to avoid spurious copper and nickel signals, TEM samples have been mounted on molybdenum grids so that spectra obtained from the silicon matrix close to the platetelet do not show significant nickel and copper signals above the bremsstrahlung background. With these precautions, the composition of pure $NiSi_2$ precipitates have been found within $\pm$ 1at% of the expected stochiometry. The accuracy of the composition is thus estimated to be $\pm$ 1at%.

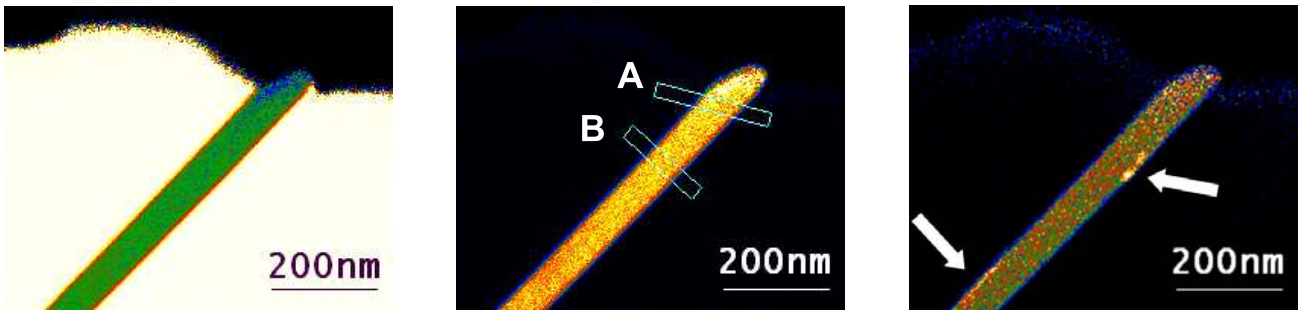

a) b) c)

Figure 5 EDX maps of the top part of a $NiSi_2$:Cu platelet displayed as relative intensities (Eq. (1)) of (a) silicon, (b) nickel, and (c) copper. Due to the Ga^+ irradiation nickel in enriched in the protruding part of the platelet at the expense of silicon. In addition, copper-rich regions inside the $NiSi_2$:Cu platelet can be seen in the copper map (arrows in (c)). The bars in (a) indicate positions of EDX linescans shown in Fig. 6. Please note, that the color code (brightness) is a semi-quantitative indication of the composition.

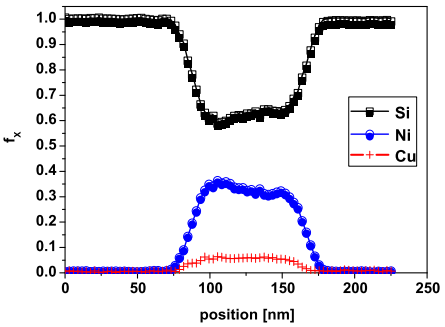

(a)

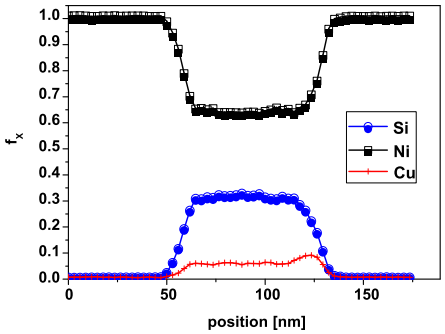

(b)

Figure 6 EDX compositional profiles calculated using Eq. (1). (a) position indicated by the bar labeled 'A' in Fig. 5a showing a higher nickel concentration at the expense of silicon in the part damaged by the 30 kV Ga^+ beam used for defect delineation. (b) position indicated by the bar labeled 'B' in Fig. 5a which includes the copper-rich region seen in Fig. 5c.

Electron diffraction and lattice imaging are consistent with face-centred cubic structure with a lattice parameter of 0.54 nm indicating the atomic structure is that of $NiSi_2$. From this it is concluded that the precipitate constitutes a solid solution of copper in $NiSi_2$ as is expected from the ternary phase diagram of the Cu:Ni:Si system [10]. Finally, it should be mentioned that the platelets are found both of type-A and type-B orientation which is parallel to the silicon matrix or in a twin-orientation with the platelet normal acting as the twin axis, respectively. Even platelets simultaneously containing both orientation variants have been observed in accord with previous works pure $NiSi_2$ platelets subjected to coarsening treatments below 800 ° [11]. Such a defect is shown as a high-resolution TEM image (Fig. 7) together with Fourier transforms from selected regions. Hence, the simultaneous presence of copper does not substantially affect the Ostwald ripening of the platelets.

The EDX map shown in Fig. 5c clearly shows two nm-sized regions with an increased copper concentration (see arrows). Both are localised inside the platelet close to the interface to the silicon matrix, as is corroborated by the profile taken along the line labeled 'B' in Fig. 5b and displayed in Fig. 6b. Such copper-rich regions may be taken as initial stages of a decomposition of the solid solution of copper in the precipitate into $NiSi_2$:Cu and Cu_3Si:Ni, where the latter refers to a solid solution of nickel in Cu_3Si [10]. One then has to conclude that at least 5at% copper can be dissolved in $NiSi_2$ at the temperature of copper in-diffusion which is 750 °C in these experiments. In addition, decomposition occurs in the solid state in these experiments as has been concluded from previous data where moderately fast cooling from high temperature has been applied [12]. In previous experiments a decomposition of an initially liquid ternary (or quaternary) alloy during cooling has been concluded [13] indicating that both processes are possible which is in accord with the ternary phase diagram of the Cu:Ni:Si system [10].

4 Conclusions In conclusion we have shown that extended defects related to transition metal impurity precipitates can be localised by chemical or ion-beam etching and subsequently subjected to TEM sample preparation using a focused on beam (FIB) system. Preferential chemical etching is successfully applied to copper-rich precipi-

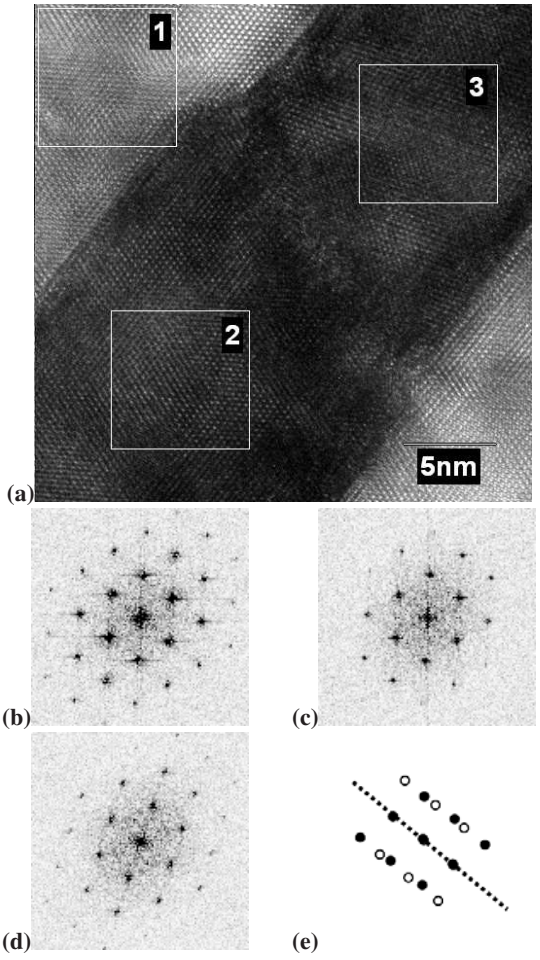

Figure 7 (a) High-resolution image of the boundary between a type-A and a type-B region inside a $NiSi_2$:Cu platelet; (b)-(d) Fourier transforms of the regions labeled '1', '2' and '3' in (a), respectively. Please note, that diffractograms (b) and (c) show the same pattern proving region 2 to be of type-A orientation. Diffractogram (d) shows the twin orientation with respect to (b) which provides evidence that region '3' is of type-B. For illustration, a scheme of the two superimposed patterns is provided in (e), where closed circles correspond to the Si matrix (and the type-A part of the platelet) and open circles correspond to the type-B part of the precipitate; in addition, the dotted line indicates the normal of the mirror plane common to both parts.

tate colonies which fails, however, in the case of nickel-rich precipitates where particles are almost completely removed by the etchant. In this case, ion beam irradiation performed *in situ* in the FIB system proofs to be a promising approach. TEM investigations of individual nickel-rich platelets reveal that surface damage from the 30kV Ga^+ irradiation comprises amorphisation of a thin silicon layer and of the top part of the $NiSi_2$:Cu platelets. In this region, the chemical composition of the particles as measured by EDX differs from that in the bulk indicating an enrichment of nickel due to selective sputtering of silicon in the $NiSi_2$:Cu compound.

Both techniques may be applicable to extended defects in semiconductors beyond metal silicide precipitates such as dislocations, stacking faults or grain boundaries. The partial damaging of the defects, however, will prevent a successful TEM analysis in case of very small defects. In this case, and also for the above defects, a combination with defect-sensitive SEM techniques as cathodoluminescence (CL) or electron-beam induced current (EBIC) should be suitable approaches.

Acknowledgements This work was financially supported by the German Federal Ministry for the Environment, Nature Conservation and Nuclear Safety and all the industry partners within the research cluster SolarFocus (0327650 B). The content of this publication is the responsibility of the authors. The authors are grateful to B. Schlieper-Ludewig and V. Radisch for technical support.

References

[1] S. A. McHugo, A. C. Thompson, A. Mohammed, G. Lamble, I. Périchaud, S. Martinuzzi, M. Werner, M. Rinio, W. Koch, H. U. Hoefs, and C. Haessler, J. Appl. Phys. **89**(8), 4282 (2001).
[2] T. Buonassisi, A. A. Istratov, S. Peters, C. Ballif, J. Isenberg, S. Riepe, W. Warta, R. Schindler, G. Willeke, Z. Cai, B. Lai, and E. R. Weber, Appl. Phys. Lett. **87**, 121918 (2005).
[3] C. Rudolf, P. Saring, L. Stolze, and M. Seibt, Mater. Sci. Eng. B, accepted for publication (2009).
[4] P. Saring, C. Rudolf, L. Stolze, and M. Seibt, Mater. Sci. Eng. B, accepted for publication (2009).
[5] F. S. d'Aragona, J. Electrochem. Soc. **119**, 948 (1972).
[6] E.Nes and J.Washburn, J. Appl. Phys. **42**, 3526 (1971).
[7] G. Cliff and G. W. Lorimer, J. Microsc. **103**, 203 (1975).
[8] J. F. Ziegler, M. D. Ziegler, and J. P. Biersack, Srim-2006.02, www.srim.org, 2006.
[9] J. F. Ziegler, J. P. Biersack, and M. D. Ziegler, SRIM The stopping and range of ions in matter (SRIM Co., 2008).
[10] E. Sokolovskaya, O. Chechernikova, E. Gladyshevskiy, and O. Bodak, Russian Metallurgy **6**, 114 (1973).
[11] M. Seibt and W. Schröter, Philos. Mag. A **59**(2), 337 (1989).
[12] M. Seibt, R. Khalil, V. Kveder, and W. Schröter, Appl. Phys. A accepted for publication (2009).
[13] T. Buonassisi, M. Heuer, A. A. Istratov, M. D. Pickett, M. A. Marcus, B. Lai, Z. Cai, S. M. Heald, and E. R. Weber, Acta Materialia **55**, 6119 (2007).